Supercontinuum fiber laser source for reflectance calibrations in remote sensing

Clarence J. Zarobila*[a,b] and Heather J. Patrick[b]

[a]Jung Research and Development Corp., Washington DC 20009 USA;
[b]National Institute of Standards and Technology, Gaithersburg MD 20899 USA

ABSTRACT

The Optical Technology Division of the National Institute of Standards and Technology (NIST) provides reference measurements of specular and diffuse reflectance of materials, including measurements that provide traceability for diffuser plaques that are used as onboard calibration standards in remote sensing. We are developing new instrumentation that will enable angle-resolved Bidirectional Reflectance Distribution Function (BRDF) measurements using a supercontinuum fiber laser-based source and a tunable monochromator. A significant improvement in optical power density at the specimen over that of lamp-based sources is expected. We present an overview of the source design and evaluation, including the predicted impact of supercontinuum sources on our next generation of BRDF measurement instrumentation.

Keywords: supercontinuum, bidirectional, diffuse, BRDF, monochromator, reflectance, STARR

1. INTRODUCTION

Supercontinuum (SC) sources[1] are broadband sources that emit directional, high power laser-like radiation in the 400 nm to 2500 nm wavelength range. Exploiting the non-linear properties in photonic crystal fiber[2] SC sources are being used in diverse applications including fluorescence microscopy,[3] chemical sensing,[4] biomedicine,[5] and hyperspectral imaging test and evaluation[6] to name a few. The Optical Technology Division of the NIST is interested in SC sources due to their potential for use in radiometric metrology applications[7] and in particular, for the calibration of the BRDF of diffuser plaques that are used as onboard calibration standards in remote sensing.

The national reference instrument for spectral reflectance measurements of spectrally neutral, non-fluorescent samples at room temperature is the NIST Spectral Tri-function Automated Reference Reflectometer (STARR).[8] Presently, STARR is limited to in-plane (meaning the sample normal, illumination axis, and receiver axis are all in a horizontal plane) measurements of BRDF. As a calibration service, STARR can measure angle-resolved BRDF from diffuse samples at wavelengths from 250 nm to 1100 nm, with total directional-hemispherical reflectance offered at wavelengths from 250 nm to 2500 nm. While the measurement of angle-resolved BRDF at Short-Wave Infra-Red (SWIR) wavelengths has been demonstrated using STARR, these measurements have been hindered by extremely low source flux at SWIR wavelengths.[9] Thus, evolving measurement demands and improvements in technology are driving the need for a new spectral BRDF facility. Among the requirements to be addressed by the new facility are improved measurement speed, on both a per angle and per wavelength basis; the capability of measuring diffuse sample, angle-resolved BRDF in the SWIR region, which is limited in the current STARR facility; and the addition of out-of-plane BRDF measurement capability which is particularly important for anisotropic samples. The goal is to perform BRDF measurements over a spectral range from 250 nm to 2500 nm, inclusive. To fulfill the need for out-of-plane measurements, the use of a five-axis goniometer is envisioned, similar to that used in the current NIST Goniometric Optical Scatter Instrument (GOSI) at the NIST Bidirectional optical scattering facility.[10]

Due to its high power, directional emission characteristics, and wide spectral emission range, an SC source appears to be particularly well-suited as an optical source for our new BRDF facility. Recently, BRDF measurements have been demonstrated with all of the SC source wavelengths illuminating the sample simultaneously, with wavelength discrimination of the scattered light using an array spectrometer.[7] This method has the potential for very fast measurement times. However, stray light and limited dynamic range in the spectrometer limit its use for high-accuracy,

*zarobila@nist.gov; phone 1 301 9758976

top-of-scale measurements. Rather, since the new system is intended to serve as a reference measurement with desired accuracies at the 0.1 % level, we couple the SC source to a monochromator, and illuminate the sample with tunable, quasi-monochromatic light. This is the same as the approach taken in STARR, except that the conventional lamp-based source is replaced by an SC source, greatly enhancing the flux at the sample and enabling the extension of angle-resolved BRDF measurements into the SWIR.

We are developing a prototype BRDF measurement system that includes an SC source, a means for the efficient introduction of light from the SC source into an imaging monochromator, and a means for projecting the quasi-monochromatic light output from the monochromator to the specimen whose BRDF is to be measured. In the prototype, the specimen will be mounted on the existing GOSI to facilitate measurements. The system is presently under construction and will be used to demonstrate the feasibility of using the SC source and related optics for the measurement of BRDF into the SWIR. In this paper, we present the prototype system design and confine any discussion of results to measurements performed to-date. Comprehensive results will be presented in the future.

2. SC SOURCE CHARACTERISTICS AND INPUT OPTICS TO MONOCHROMATOR

The source for our prototype BRDF measurement system is a Fianium[#] SC400-4.[11] The spectral radiance distribution $L(\lambda)$ of this laser source was measured by directing its output into an 20.32 cm (8") diameter integrating sphere coated with spectralon, and measuring the sphere wall radiance using a spectroradiometer. The results are shown in Figure 1.
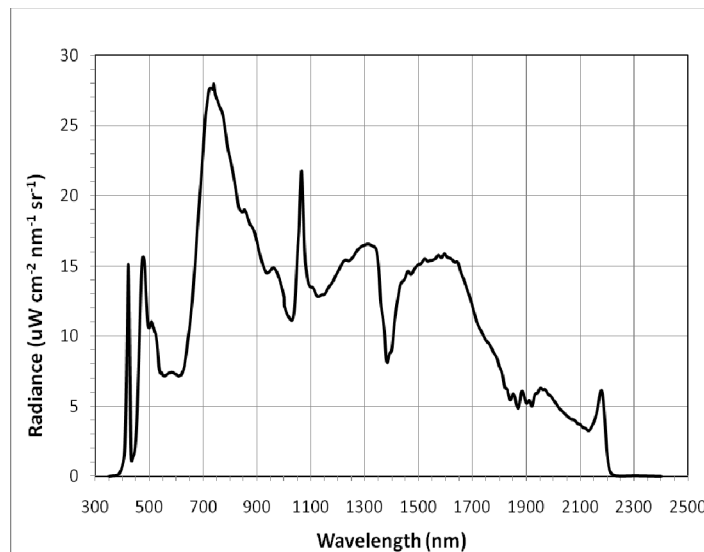

Figure 1. Spectral radiance of sphere wall

Note the relative lack of energy below approximately 400 nm. This characteristic is typical of an off-the-shelf SC source and therefore the final BRDF measurement system may ultimately include an additional source, such as a Quartz-Tungsten-Halogen (QTH) lamp, to cover the UV and a portion of the visible wavelengths. At the other end of the spectrum in the SWIR, it is anticipated that a SWIR-enhanced version of the SC source will result in coverage out to 2500 nm.

The flux density of the source, $\varphi(\lambda)$, is calculated from[12]

$$\Phi(\lambda) = L(\lambda)\pi A_s / M(\lambda) \tag{1}$$

where A_s is the surface area of the sphere, and $M(\lambda)$ is the sphere multiplier given by

$$M(\lambda) = \rho(\lambda)/[1 - \rho(\lambda)(1 - f)]. \tag{2}$$

In Eq. (2), $\rho(\lambda)$ is the sphere wall reflectance, and the port fraction f is the sum of the area of the entrance and exit ports divided by A_s. Eqs. (1) and (2) along with the measured values for $L(\lambda)$ and the sphere characteristics can be used to calculate the flux density. Table 1 shows the results of the calculations. As can be seen, the calculated flux density from this SC source is indeed very high, on the order of mW/nm, throughout most of the spectral range.

Table 1. Flux density measurements.

Wavelength (nm)	ρ	M	Flux Density (mW/nm)	Wavelength (nm)	ρ	M	Flux Density (mW/nm)
450	0.99	28.18	0.46	1100	0.99	28.18	1.96
500	0.99	28.18	1.56	1200	0.99	28.18	2.11
550	0.99	28.18	1.05	1300	0.99	28.18	2.38
600	0.99	28.18	1.05	1400	0.99	28.18	1.38
650	0.99	28.18	1.57	1500	0.99	28.18	2.18
700	0.99	28.18	3.41	1600	0.99	28.18	2.27
750	0.99	28.18	3.89	1700	0.98	21.83	2.25
800	0.99	28.18	3.26	1800	0.98	21.83	1.46
850	0.99	28.18	2.73	1900	0.98	21.83	1.01
900	0.99	28.18	2.40	2000	0.97	17.76	1.25
950	0.99	28.18	2.13	2100	0.94	11.21	1.33
1000	0.99	28.18	1.81	2200	0.96	14.91	0.54

Our SC400-4 has been shipped with a collimator factory-installed onto the end of the single-mode photonic crystal fiber. The lens (or lenses) within the collimator also serve to protect the end of the fiber. The laser-like, collimated output of the SC source means that unlike a conventional lamp, all of the flux from the SC source can be coupled into the monochromator, given an efficient means to focus the beam waist to the entrance slit and to insure that the beam divergence at all wavelengths is less than the acceptance angle of the monochromator. In our prototype system, this consists of a converging lens pair designed and positioned such that 1) the image of the beam waist is formed at the monochromator entrance slit, and 2) the divergence of the beam at the entrance slit is constant for any wavelength, and this value is less than the acceptance angle of the monochromator. To achieve these characteristics, reflective optics can obviously be used. But in the interest of speed in procurement, refractive optics were selected. The collimator and lens pair design are discussed in detail below.

2.1 Collimator measurements and input optics modeling

To design a system that provides efficient coupling of the near-Gaussian polychromatic laser light exiting the collimator to the monochromator entrance slit, it is necessary to examine the degree of collimation vs. wavelength, and measure the size of the beam exiting the collimator. It is known that the beam divergence at the output of photonic crystal fiber varies with wavelength[13] and therefore a varying beam size and limited spectral range for the collimation are expected since glass lenses are employed within the collimator. Several approaches to measure the beam size are available, including the coaxial aperture method, the translating knife-edge method, or the use of interference filters and a Charge-Coupled Device (CCD) camera or commercial beam profiler. The former two methods require additional optical components such as an integrating sphere and calibrated spectrograph (which has the advantage of a continuum of wavelength measurement), while the latter two approaches are relatively simple but dependent upon the bandwidth of the interference filters (and the disadvantage of only discrete wavelength measurement). All approaches are limited by the spectral range of the spectrograph/detector or beam profiler. We have employed three out of the four approaches and in the interest of brevity, discuss only the first approach herein.

The collimator was mounted on an optical rail, and a coaxial aperture 1.5 mm in diameter was positioned at z = 30.48 cm (12") from the collimator. The aperture could be translated slightly in directions at right angles to the beam to maximize transmitted power. The integrating sphere was located behind the aperture, and a calibrated fiber-optic probe coupled to a spectrograph was used to monitor the sphere wall radiance. The wall radiance in the absence of the aperture defines a maximum; the wall radiance with the aperture in place divided by the maximum define a transmission, *T(z)*, through the aperture. The beam size at z, *w(z)*, is calculated from[14]

$$w(z) = \{-2r^2/\ln[1 - T(z)]\}^{1/2} \qquad (3)$$

where r is the radius of the aperture. The aperture was repositioned to z = 60.96 cm (24") from the collimator, and *w(z)* was calculated. Table 2 gives the results for *w(z)* at the two rail positions for selected wavelengths.

Table 2. Beam size from collimator at selected wavelengths

Wavelength (nm)	w(30.48 cm) (mm)	w(60.96 cm) (mm)	Wavelength (nm)	w(30.48 cm) (mm)	w(60.96 cm) (mm)
450	0.95	0.75	1400	2.14	2.95
500	0.93	0.69	1500	2.40	3.36
600	0.80	0.66	1600	2.69	3.77
700	0.99	0.78	1700	2.99	4.13
800	1.15	0.96	1800	3.23	4.52
900	1.34	1.30	1900	3.43	5.03
1000	1.50	1.64	2000	3.76	5.56
1100	1.70	2.01	2100	4.06	5.99
1200	1.86	2.27	2200	4.23	6.81
1300	2.05	2.63			

It is evident that the beam converges below 1000 nm, and diverges from 1000 nm to 2200 nm. The beam size increases with wavelength and without subsequent beam shaping optics, a relatively large loss should be expected if the light from the collimator falls directly onto the entrance slit of a monochromator. Alternatively, if a single focusing optic were used in an attempt to image the waist to the entrance slit, the beam waist position, divergence, and beam size on the first collection mirror of the monochromator would vary greatly with wavelength, which would also lead to excess loss at some wavelengths. Thus for efficient coupling, the subsequent converging lens pair must image the beam to a size less than the width of the entrance slit, and whose divergence is less than the acceptance angle of the monochromator optics.

The collimator was modeled using the data in Table 2 and the ZEMAX optical design program[15] in the Physical Optics Propagation (POP) mode. In POP mode, Gaussian or higher order laser beams may be defined. Among other properties, beam size, amplitude, phase, intensity, and Rayleigh range may be computed. In the present problem, beam size at two locations and wavelength are known, and it is a relatively simple matter to use ZEMAX to model the collimator. The beam itself is defined to originate from an object (a 2.5 μm waist at the end of the photonic crystal fiber) and a paraxial surface type having a variable focal length *FL(λ)* at variable distance *D1(λ)* from the waist is used to represent the collimator. The ZEMAX operand "GBPS", the Gaussian Beam Paraxial Size operand, is defined in the merit function such that the measured beam size given in Table 2 is obtained at 30.48 cm and 60.96 cm from the paraxial surface (the collimator). Table 3 summarizes the results for the ZEMAX model. It should be noted that these results do not represent the actual properties of the fiber and collimator, as in fact the true beam waist varies with wavelength, and in the collimator, *D1* is a constant. Rather, they are a convenient model that reproduces the measured divergence versus wavelength.

Table 3. Collimator model parameters

Wavelength (nm)	D1 (mm)	FL (mm)	Wavelength (nm)	D1 (mm)	FL (mm)
450	20.05	19.83	1400	7.44	7.55
500	18.38	18.15	1500	7.59	7.72
600	12.49	12.41	1600	7.89	8.03
700	13.51	13.40	1700	8.51	8.66
800	13.26	13.17	1800	8.48	8.64
900	12.10	12.09	1900	7.56	7.73
1000	10.73	10.76	2000	7.66	7.84
1100	9.88	9.95	2100	7.95	8.15
1200	9.51	9.59	2200	5.91	6.10
1300	8.88	8.99			

Note that the object distance (*D1*) is always slightly outside the focal length (*FL*) of the collimator below 1000 nm, a characteristic consistent with the expectation of a converging beam. On the other hand, D1 is inside the focal length at 1000 nm and above, a characteristic consistent with a diverging beam.

The next step is to design and model a pair of translatable converging lenses such that for any wavelength, the image of the beam waist can be formed at the entrance slit of the monochromator, and the divergence of the beam at the entrance slit can be set to the target divergence angle for the monochromator (discussed below.) A sketch of the concept is shown in Figure 2. The first surface of the initial lens is located 304.8 mm (12") from the collimator.
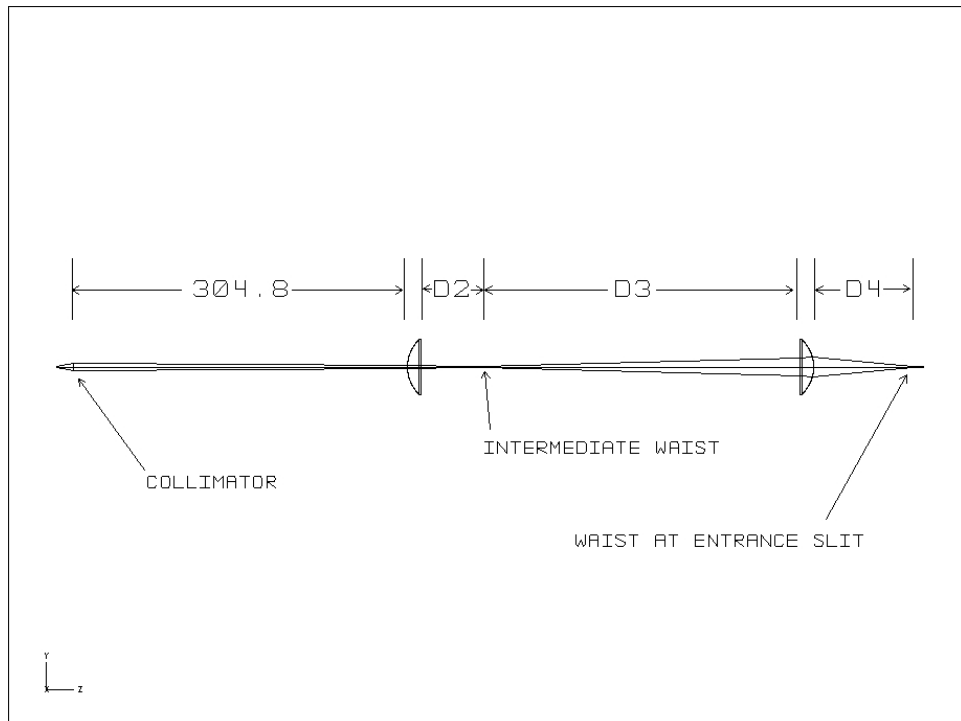

Figure 2. Raytrace of Input Optics Concept

The lenses and collimator are mounted on the optical rail so that the distance *D2 + D3*, and distance *D4*, may be varied vs. wavelength to optimized rail positions yet to be calculated. Optimized positions will vary with wavelength due to the change in beam size and the chromatic variation in lens power (focal length). Plano-convex (PCX) lenses are selected because of their off-the-shelf availability in optical glass types (e.g., fused silica or CaF_2) suitable for use over a wide wavelength span from the UV into the SWIR. Their focal length is selected as follows. First, note that the first lens is used to converge a quasi-collimated beam to an intermediate waist located at D2. Any reasonable focal length suitable for use on an optical rail, e.g., in the range 50-100 mm, is sufficient, and the lens diameter should be greater than 5 times the worst-case beam size (about 6 mm at 2200 nm) to collect > 99.999% of the light and to mitigate diffraction effects. The second lens must be positioned so that its object (the intermediate waist) is outside the lens' focal length so that the light converges again to form the image of the waist at the entrance slit. It should not have too long a focal length otherwise the optimum position of the lens might occur at a location off the rail. Furthermore, the diameter of the lens must be large enough to once again collect all of the light and to prevent diffraction effects. Thus, a 75 mm focal length was chosen for both lenses and a search of vendors resulted in the selection of a 12.7 mm thick fused silica optic having diameter of 50 mm, more than sufficient to satisfy the 5 times rule-of-thumb. The radius of the spherical surface is 34.38 mm. Both lenses were purchased uncoated.

The monochromator in our prototype system is a McPherson Model 218. This imaging instrument employs a criss-cross Czerny-Turner design with a focal length of 300 mm and 50 mm x 50 mm ruled grating and mirrors. Using the 5 times rule-of-thumb once more, this time for the ratio mirror size/beam size, the beam should not have a size (radius) greater than 10 mm on the mirror. Since the focal length is 300 mm, the corresponding divergence angle is $\theta = \tan^{-1}(10/300)$, or 0.033 radians. This is the target divergence angle to use at the entrance slit of the monochromator, and is well within the instrument's f/5.3 acceptance cone. The path length from grating to exit slit is about 545 mm.

The ZEMAX optical design program was again employed, this time to calculate positions *D2*, *D3*, and *D4* versus wavelength such that the image of the waist occurs at the entrance slit and so that divergence of the waist at the entrance slit is 0.033 radians for that wavelength. The steps to achieve this are as follows:

a) Set up the ZEMAX Lens Data Editor (LDE) to include a paraxial surface type (the model collimator) and one PCX lens. Enter the FL and D1 data given in Table 3 into the LDE for the paraxial surface, and enter the radius and thickness data for the fused silica lens located 304.8 mm (12") from the paraxial surface. Set up ZEMAX to compute at 450 nm.

b) Set up a merit function and use the "GBPP" (Gaussian Beam Paraxial Position) operand, target = 0, on the last surface in the LDE. This is the intermediate waist location. Make this position variable. Input an initial waist w_0 equal to 2.5 μm (the "radius" of the photonic crystal fiber) at 450 nm into the merit function and optimize.

ZEMAX will find the value of *D2* to satisfy the merit function target GBPP = 0 at 450 nm. Recompute and record *D2* for all the other wavelengths and data in Table 3.

The next task is to compute *D3* and *D4*. To do this, these steps are followed:

c) Add the second PCX lens to the LDE and at a seed location of 100 mm from the first lens. Make this position variable. Add a seed image location of 100 mm, and make this position variable as well.

d) Enter the *D2* data for 450 nm into the LDE.

e) Set up a new merit function and use operands GBPP and "GBPD" (Gaussian Beam Paraxial Divergence) to force the image of the waist to be located at the last (image) surface and to have a target divergence equal to 0.033 radians. Optimize the system.

ZEMAX will compute locations *D3* and *D4* to satisfy the target divergence of 0.033 radians at 450 nm. A further benefit is the beam size at the entrance slit (or anywhere else) may be computed. Steps d) through e) are repeated for every other wavelength in Table 3.

Table 4 summarizes the results of the optimization process. The waist at *D4* ranges from about 4.3 μm at 450 nm to about 20 μm at 2200 nm, values very much less than the typical width of an entrance slit. This implies that the entrance slit in this system can be considered to be the size of the waist (or rather, 3 to 5 times the waist). The waist at the entrance slit is subsequently imaged to the exit slit by the monochromator optics. The divergence angle, θ, is calculated from $\theta = \tan^{-1}[w(D4)/Rayleigh\ Range]$ and it is equal to the target value. As an example, if a wavelength of 800 nm

were desired to be output from the monochromator, the optimized input optic positions would be $D2 = 64.01$ mm, $D3 = 226.53$ mm, etc.

Table 4. Results for the ZEMAX model of the PCX converging lens system

Wavelength (nm)	D2 (mm)	D3 (mm)	D4 (mm)	w(D4) (mm)	Rayleigh Range (mm)	Divergence angle at D4 (rads)
450	61.61	247.23	103.80	4.304E-03	0.1293	0.0333
500	61.26	252.24	104.00	4.782E-03	0.1437	0.0333
600	63.03	289.93	100.26	5.738E-03	0.1724	0.0333
700	62.97	248.96	106.81	6.695E-03	0.2012	0.0333
800	64.01	226.53	111.92	7.652E-03	0.2299	0.0333
900	66.77	209.81	116.76	8.609E-03	0.2587	0.0333
1000	69.34	199.96	120.34	9.566E-03	0.2875	0.0333
1100	71.51	188.34	125.12	1.052E-02	0.3163	0.0333
1200	72.47	179.47	129.53	1.148E-02	0.3450	0.0333
1300	74.07	171.71	134.07	1.244E-02	0.3738	0.0333
1400	76.53	170.99	135.07	1.339E-02	0.4026	0.0333
1500	77.19	159.89	142.18	1.435E-02	0.4314	0.0333
1600	77.61	151.93	150.13	1.531E-02	0.4602	0.0333
1700	77.37	143.71	158.61	1.627E-02	0.4890	0.0333
1800	78.02	139.01	165.05	1.723E-02	0.5179	0.0333
1900	80.05	136.89	168.89	1.818E-02	0.5466	0.0333
2000	80.74	132.00	177.24	1.914E-02	0.5755	0.0332
2100	80.94	127.97	185.54	2.010E-02	0.6043	0.0332
2200	84.99	128.57	186.01	2.105E-02	0.6330	0.0332

2.2 Validation of input optics concept

To validate the input optics concept, measurements of the beam size and divergence after propagating through the converging lens pair were performed. The SC collimator, lenses, and a filter wheel were installed on an optical rail, as shown in Figure 3 below. Interference filters were installed in the filter wheel to wavelength-select a nominal 10 nm Full-Width Half-Max (FWHM) bandwidth in the light exiting the collimator. The data in Table 4 was transferred to a spreadsheet to facilitate the calculation of the lens positions from a reference point. To measure the size and divergence of the beam, a beam profiler (Thorlabs BP109-VIS) was located behind the second lens and translated in 5 mm increments from the rear of the second lens, through the minimum, and then beyond. In this manner, the beam size could be measured vs. rail position and the divergence angle calculated.

Figure 4 shows a plot of the beam size and divergence results obtained at 450 nm when the lenses were positioned at their optimum locations on the rail. Note that the beam size, W, reaches a sharp minimum and that the slope beyond the minimum is equal to 0.033 mm/mm, the value of the target divergence. Similar results were obtained at the other interference filter center wavelengths, thus validating the input optics concept.
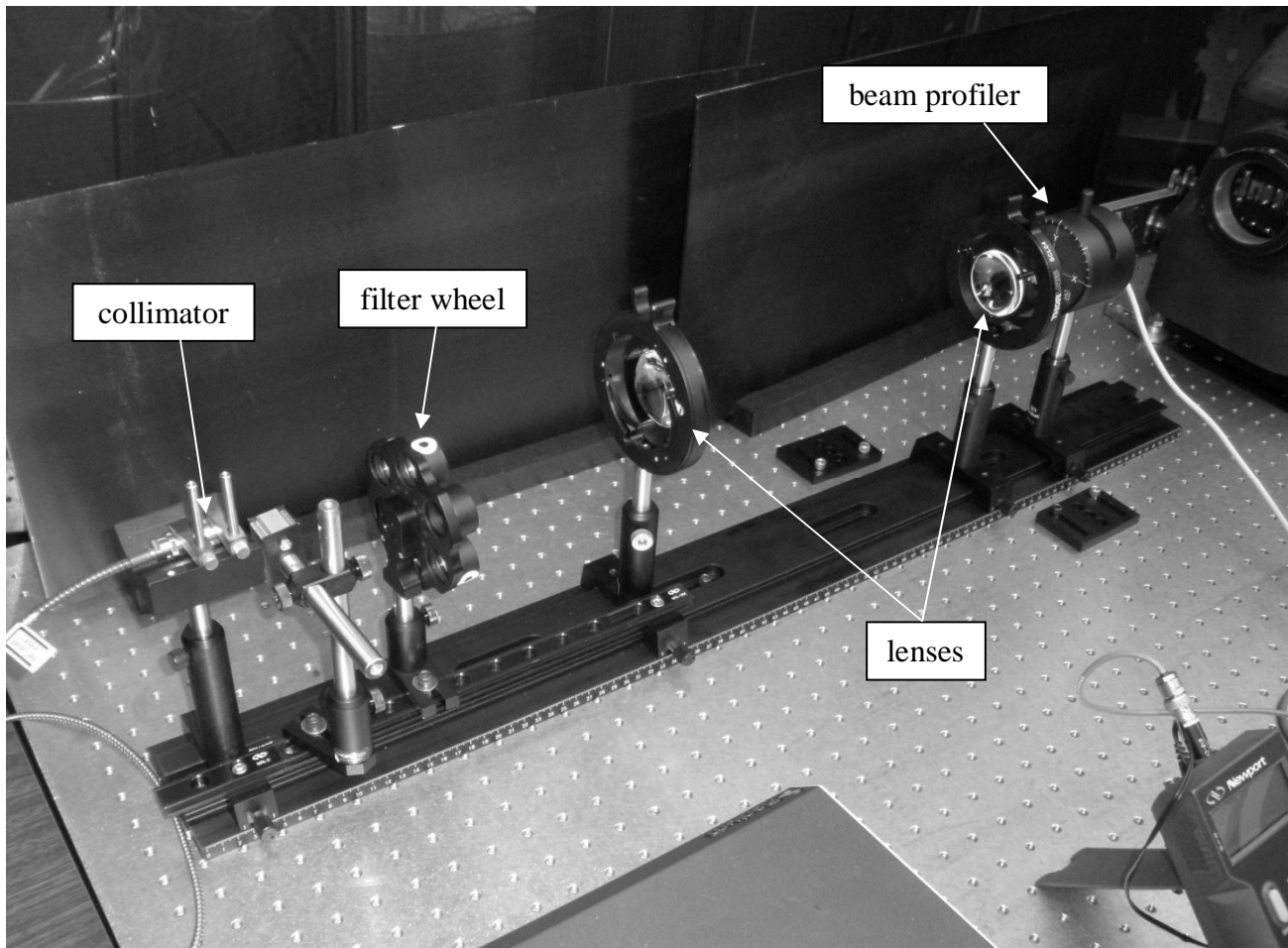
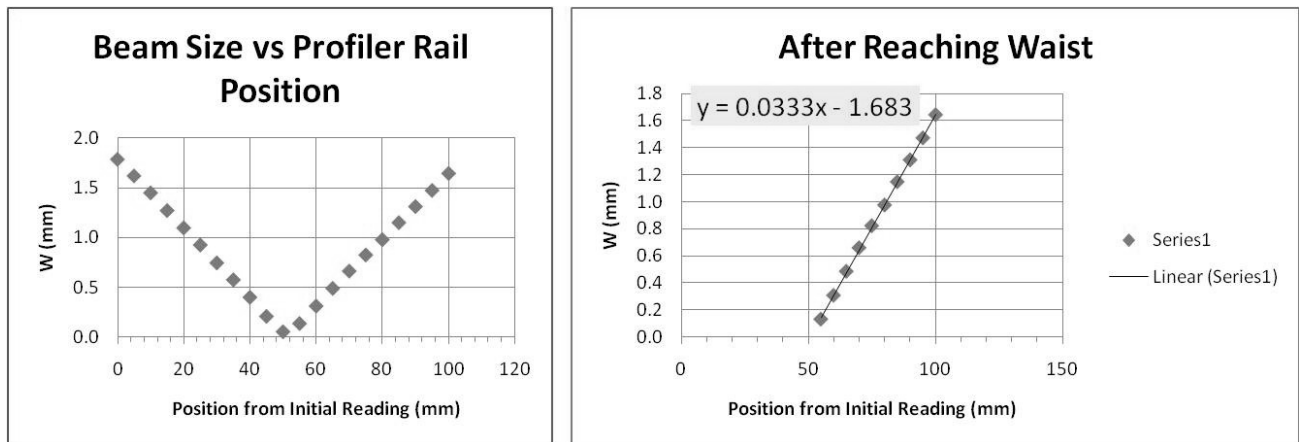Figure 3. Photograph of prototype system input optics

Figure 4. Experimental results near entrance slit location for beam size and divergence at 450 nm

Etendue issues when coupling to the monochromator are obviously minimized because of the SC laser source, and our approach. It would be a simple matter to transfer the computed positions to optical rail positions and to manually locate the lenses, or to automate their positioning using a motorized system if required. The advantage of this is that for any desired output wavelength, the beam waist and divergence are optimized specifically for this wavelength. However, based on our modeling, we believe that a fixed lens position appears to be adequate to cover all wavelengths, thus considerably simplifying the coupling of the light to the monochromator. Refer to Sections 2.3 and 2.4 below.

2.3 Effect of lens position on monochromator performance

In order to compare the transmitted power and output bandwidth of the monochromator when the lenses are at their optimized locations to the results obtained when the lenses are at a fixed location, we model a virtual monochromator working at three representative wavelengths, 500 nm, 1200 nm, and 2000 nm. Suppose it employs a grating having a line density of 1200 l/mm for use at 500 nm, another grating having a line density of 600 l/mm for use at 1200 nm, and a third grating having a line density of 300 l/mm for use at 2000 nm. All gratings operate in the first diffraction order. Further suppose the monochromator is coupled to the SC source collimator and converging lens pair as shown in Figure 5. Assume light from the collimator is unpolarized. Let the mirrors and gratings be modeled as simple aluminum reflectors (neglect the absolute efficiency of the gratings), and let the exit slit be modeled as a rectangular aperture 1 mm wide by 4 mm high. ZEMAX may be used once again in POP mode, this time to compute the beam size, the waist, the
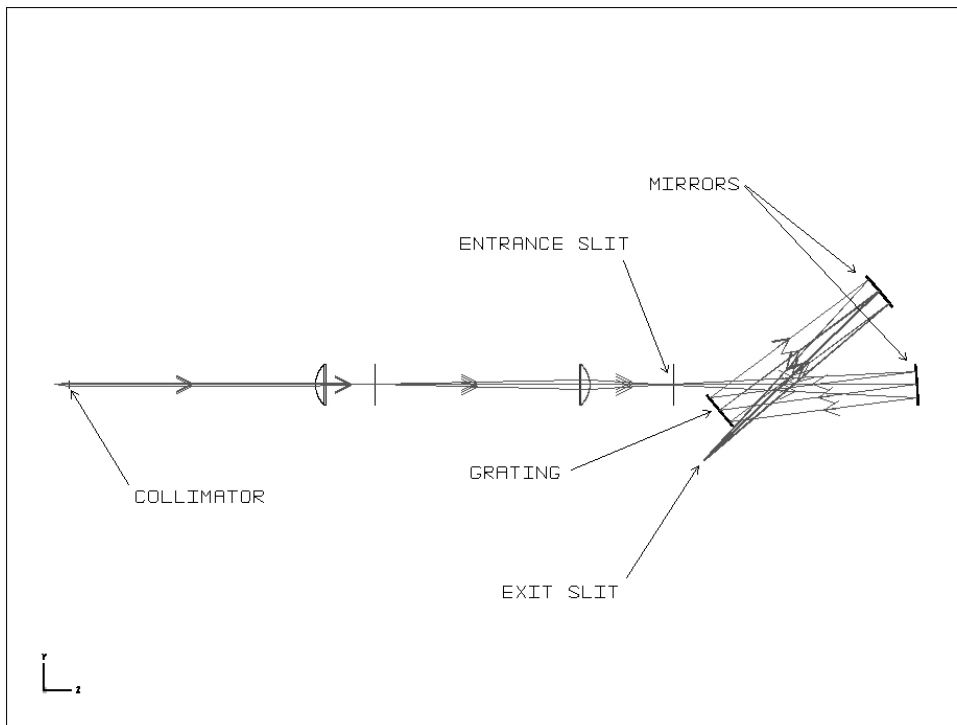

Figure 5. Raytrace of collimator coupled to monochromator

Rayleigh Range, and the transmitted power through the exit slit as a function of wavelength. Plots of the bandwidth of the light at the exit slit may also be generated.

Figure 6 shows a plot of the virtual power transmitted through the 1 mm wide slit at 1200 nm when the lenses are located at the optimum position and when they are fixed at the 2200 nm position. The 2200 nm position was chosen for the fixed lens case because in this configuration, the divergence of the beam at the monochromator's input slit is optimized at the target divergence for 2200 nm, and is less divergent for all other wavelengths. This insures that the monochromator

mirrors and grating will be underfilled for all wavelengths. The plot takes into account the transmission through the lenses and the reflection from the aluminum surfaces (but not the efficiency of the grating). The bandwidth of the light exiting the monochromator results from the convolution of the polychromatic input spectrum, the image of the waist at the entrance slit, and the Instrumental Line Profile (ILP) of the monochromator. The ILP is the response of the monochromator to monochromatic input light. The ILP is generally a function of the width of the entrance and exit slits, the dispersion, aberrations, and the quality of the optical components and their alignment. The FHWM of the function is calculated to be equal to 5.14 nm and 5.38 nm at the optimum and 2200 nm positions, respectively. Operating at the 2200 nm position tends to smooth the bandwidth function and allows light through from wavelengths further away from the center wavelength, effects similar to those expected of a defocus. This is reasonable given that the beam waist will only be located precisely at the exit slit for 2200 nm. The fraction of power through is about the same in both cases, suggesting the beam size at the exit slit is much less than the width of the exit slit (1 mm) regardless of lens position. Table 5 summarizes results for the three representative wavelengths when the lenses are located at their optimized positions, and at the 2200 nm positions. From these results, we conclude that positioning the lenses at the 2200 nm location has no deleterious effect since the beam size is always very much less than the width of the exit slit width at the test wavelengths.
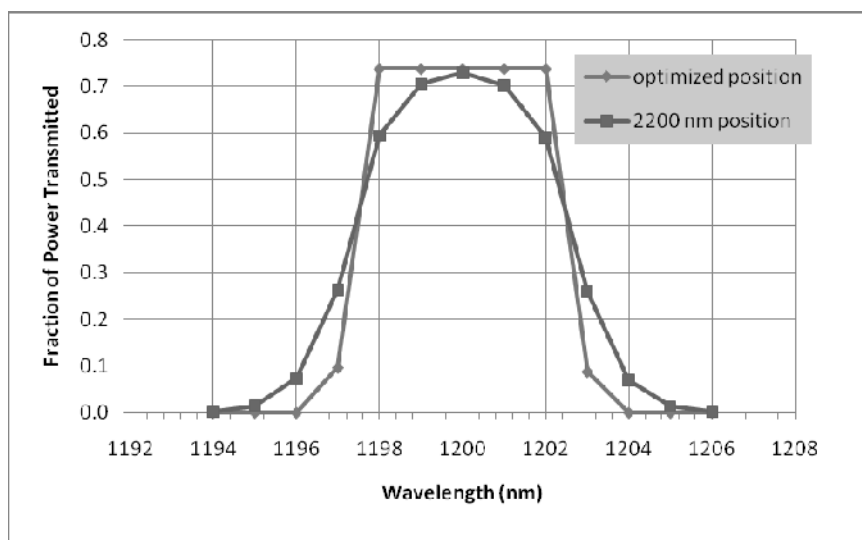

Figure 6. Plot of virtual power transmitted through 1 mm x 4 mm slit

Table 5. ZEMAX modeling results at 1 mm x 4 mm exit slit

Parameter	optimized	optimized	optimized	at 2200 nm	at 2200 nm	at 2200 nm
	500 nm	1200 nm	2000 nm	500 nm	1200 nm	2000 nm
beam size at exit slit (mm)	0.006	0.011	0.018	0.305	0.332	0.132
divergence angle (rads)	0.036	0.037	0.036	0.012	0.024	0.034
FWHM (nm)	2.87	5.14	10.48	2.81	5.38	10.84

We propose to use a large core optical fiber having a core diameter of 1.8 mm and an Numerical Aperture (NA) of 0.22 as the "exit slit" to collect light and to deliver it to the projection optics (to be discussed in Section 3 below). This is more than 5 times greater than the beam size at 1200 nm and will also result in a greater bandwidth. Refer to Figure 7 for a comparison plot showing the increase in bandwidth using the fiber vs. that obtained for the 1 mm slit. The FWHM is

calculated to be 9.63 nm, a value almost 1.8 times that obtained for the 1 mm slit. Along with geometric positioning flexibility, another benefit of using such a fiber is spatial averaging and the removal of "hot spots" in the light which is to be projected to the specimen.
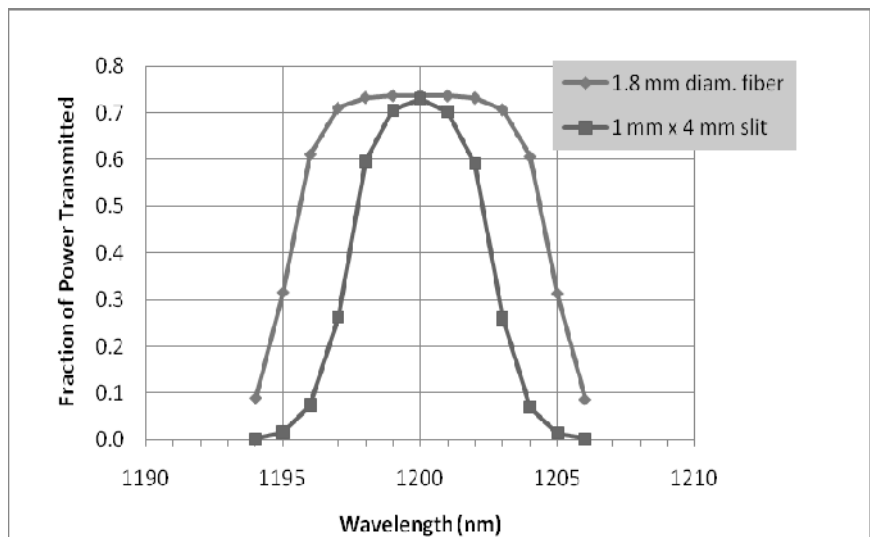

Figure 7. Plot of virtual power transmitted through 1.8 mm fiber and 1 mm x 4 mm slit

2.4 Measurements of monochromator efficiency with fixed input optics

The discussion in Section 2.2 neglected the efficiency of the gratings(s). To examine the throughput of the monochromator and determine the efficiency at selected wavelengths, several interference filters were installed at the output of the collimator. Each had a different center wavelength. The light was directed into the monochromator through the converging lens pair set to the 2200 nm position. For unpolarized light, the power through the filters at the input to the monochromator entrance slit was compared to the power measured out of the exit slit when the monochromator was tuned to the center wavelengths of the interference filters. The bandwidth of the light was also measured at the input and output of the monochromator by picking off a portion of the light with a thin glass plate and directing the light to an integrating sphere coupled to a calibrated spectrograph. The exit slit was adjusted to 2 mm, a width consistent with a 5 nm bandwidth when using a 1200 l/mm grating. Table 6 gives the results of the measurements. The estimated standard uncertainty (Type B) in the measurement of power and bandwidth is 1 % and 0.2 nm, respectively. The estimated expanded uncertainty (coverage factor k = 2) in the efficiency is given in the last column.

Table 6. Monochromator efficiency at selected interference filter wavelengths

Center Wavelength (nm)	Power at entrance slit (mW)	FWHM at entrance slit (nm)	Power density (mW/nm)	Power at exit slit (mW)	FWHM at exit slit (nm)	Power density (mW/nm)	Efficiency	Expanded Uncertainty in Efficiency
450	1.14	6.64	0.17	0.12	4.57	0.026	0.153	0.017
532	7.00	8.06	0.87	1.39	5.24	0.26	0.305	0.029
580	5.65	9.80	0.58	0.98	5.20	0.19	0.327	0.030
710	21.8	8.94	2.44	3.54	5.08	0.70	0.286	0.027

It is also important to consider the polarization of the light exiting the monochromator. In the BRDF measurement system, it is desirable to be able to select any linear polarization state to project to the sample. The easiest way to achieve this is to install a rotatable linear polarizer after the monochromator output (see Section 3 below). While the SC source is unpolarized, the monochromator output can become polarized if the grating efficiency is highly polarization dependent, leading to large differences in flux to the sample with the polarizer rotation angle. We have measured the change in flux with polarizer angle for the wavelengths shown in Table 6, and for 532 nm, 580 nm, and 710 nm, there was less than 20 % variation. This is generally the case when ruled gratings are used near their blaze wavelength. However, at 450 nm, the variation was 76 %, suggesting 450 nm is far removed from the grating's blaze wavelength. The measurements in Table 6 and the examination of commercially available grating efficiency curves suggests that an overall efficiency of about 30 % is a good representative number to use in any subsequent modeling, but the gratings must be carefully chosen for low polarization dependence over their operating wavelengths.

3. OUTPUT OPTICS

The quasi-monochromatic light exiting the monochromator must be collected and delivered to a specimen that is remotely located, ultimately several meters from, the exit slit of the monochromator. To facilitate the projection of this light, we are investigating the use of a large core optical fiber to collect the light exiting the monochromator, and reflective optics in a finite-conjugate Newtonian telescope arrangement to deliver the light to the specimen. Refer to the ZEMAX raytrace shown in Figure 8.
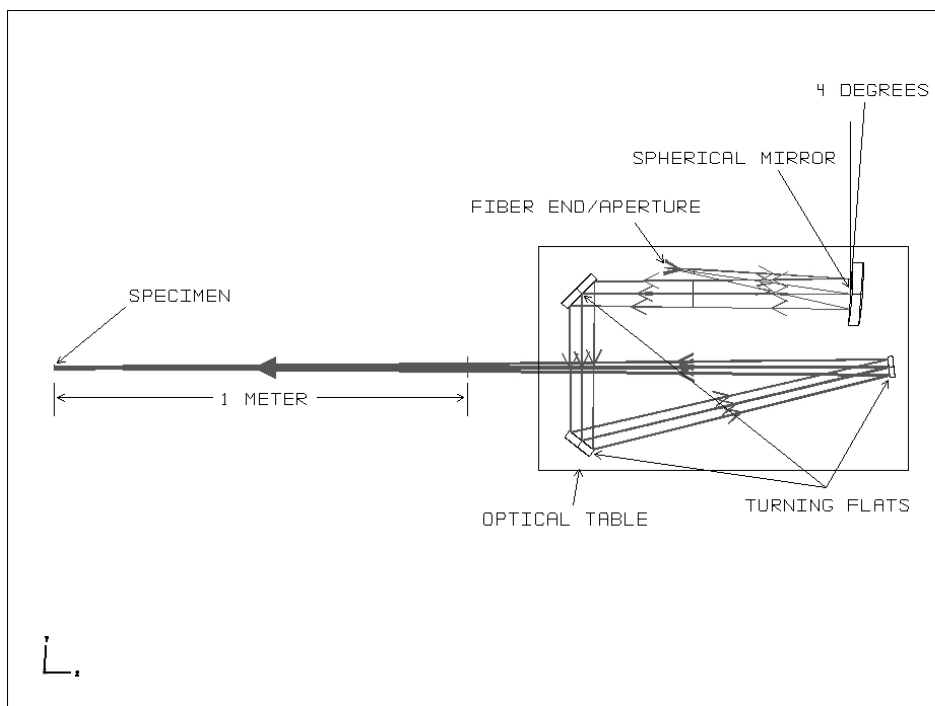

Figure 8. ZEMAX raytrace of prototype projection optics

A candidate fiber is the CeramOptec Optran WF series silica/silica step-index fiber.[16] The large core (1.8 mm) acts as the exit slit of the monochromator. The reciprocal linear dispersion of the monochromator multiplied by the fiber core diameter sets the effective bandwidth of the light. The NA of the fiber is 0.22, corresponding to an acceptance angle of 12.7°, an angle very much greater than the divergence angle in the light at the output of the monochromator (see Table 5). The fiber's optical loss for a 1 meter length is approximately 0.04 dB from about 400 to 2000 nm, then increases to about 0.2 dB at 2200 nm. Light exiting the fiber floods a precision aperture located a few mm from the end

of the fiber. The diameter of the precision aperture (1.5 mm) is less than that of the fiber (1.8 mm), and the aperture is the object to be imaged by the subsequent optics. The transmission through the aperture is estimated to be 70 % (using ZEMAX) when the aperture is located a few mm from the end of the optical fiber. The aperture is positioned at the focus of an off-the-shelf protected-aluminum first-surface spherical mirror whose radius of curvature is 812.8 mm. The fiber end, aperture, and spherical mirror are all inclined at an angle of 4 degrees as shown. The tilt introduces aberrations which will be addressed in the future, perhaps by substituting an off-axis ellipsoidal mirror for the spherical mirror. The diameter of the spherical mirror very much exceeds the cross-section of the beam exiting the fiber. The light reflected by the spherical mirror slowly converges to a nominal 1 cm diameter spot on the specimen along a path that is turned by three protected-silver mirror flats kinematically mounted. The specimen is located on the existing GOSI approximately one meter from the end of the optical table.

The schematic shown in Figure 9 gives more detail in the output optics. An optical chopper coupled to a lock-in amplifier provides synchronous demodulation capability. This chopper may be located either after the last turning mirror or in the input optics prior to the monochromator. A polarizer is included to adjust the polarization state of the light incident on the specimen, as discussed above. The last element in the optical train prior to the sample mounted on the goniometer is a beam pick-off (UV grade fused silica wedge) that is used to provide a reference. Because absolute measurements of the light flux are required for BRDF measurements, the diameter of the precision aperture and the power of the spherical mirror are selected so that the footprint of the beam is entirely contained within the existing 25.4 mm diameter GOSI receiver head that is located 590 mm behind the specimen when absolute flux measurements are made. It is expected that the future system will instead require a one meter length receiver arm, and therefore the projection optics and the final system receiver must be designed with this requirement in mind.
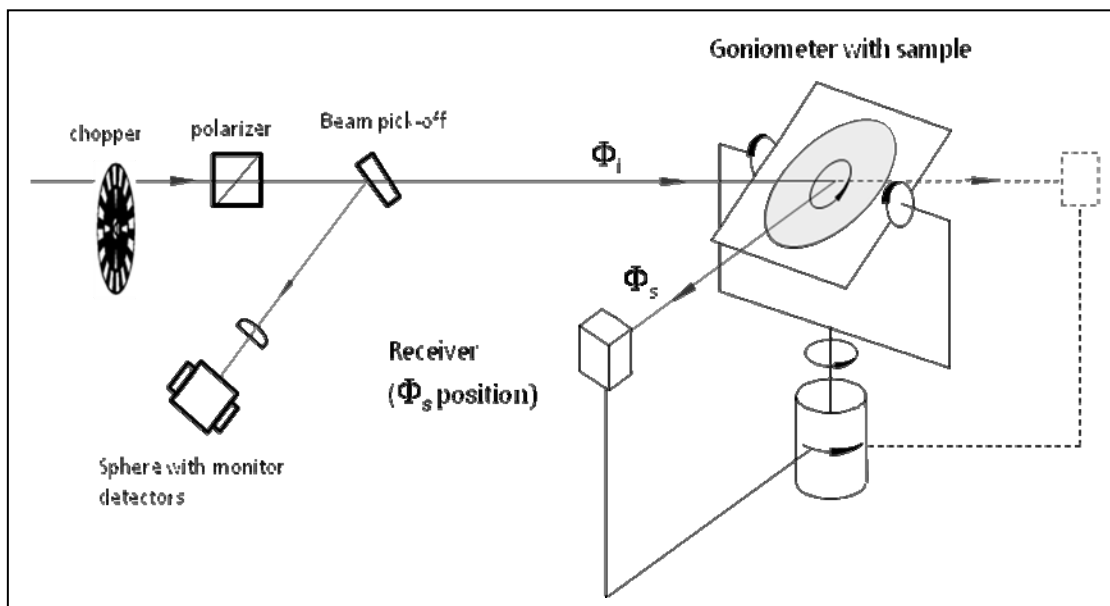

Figure 9. Schematic of output optics prior to and including specimen

4. ANTICIPATED FLUX DENSITY ON SPECIMEN

Based on the above measurements and ZEMAX modeling, and loss data published for the optical fiber, it is possible to assemble a table that contains estimates for the fraction of power transmitted when propagating through or reflecting from the optical components in the prototype system. The product of the loss terms gives the estimated throughput.

Multiplying the estimated throughput by the measured SC source flux density (Table 1 herein) results in the estimated flux density on the specimen. Table 7 below summarizes these estimates at selected wavelengths.

Table 7. Estimated throughput and flux density on specimen in prototype system at selected wavelengths

Parameter	500 nm	1000 nm	1500 nm	2000 nm	2200 nm
Input optics (converging lens pair)	0.87	0.87	0.87	0.88	0.88
Order-sorting filter transmission	1.00	0.85	0.85	0.85	0.85
Monochromator throughput	0.30	0.30	0.30	0.30	0.30
Fiber (absorption and end loss) transmission	0.91	0.91	0.91	0.91	0.88
Transmission through aperture	0.70	0.70	0.70	0.70	0.70
Mirrors (4 total, 3 protected Ag, 1 protected Al)	0.91	0.88	0.87	0.86	0.86
Chopper	0.50	0.50	0.50	0.50	0.50
Polarizer	0.50	0.50	0.50	0.50	0.50
Beam pick-off (fused silica wedge)	0.93	0.93	0.94	0.94	0.94
Total throughput fraction	**0.04**	**0.03**	**0.03**	**0.03**	**0.03**
Source flux density, Table 1 (µW/nm)	1560	1810	2180	1250	540
Flux density to specimen (µW/nm)	**55**	**52**	**63**	**36**	**15**

The existing STARR uses a 100 W Quartz-Tungsten Halogen (QTH) lamp focused into a single-grating monochromator. At 1000 nm, the output power from the monochromator is about 1 µW in a 14 nm bandwidth[9], corresponding to a flux density of 0.07 µW/nm. As can be seen from the 1000 nm data above, the improvement expected in flux density by using the SC source over the flux density in STARR is a factor of about 52/0.07, or > 700 at 1000 nm.

5. ANTICIPATED FLUX ON DETECTOR

Assume a specimen is mounted on a goniometer and irradiated with quasi-monochromatic light having incident signal power S_i. A radiometer is used to detect the reflected signal from the specimen. Let the reflected signal be denoted as S_r. The reflectance factor, R, of the specimen when broadband detection is used is given by Eq. (1) of Reference 9. The equation is

$$R = (\pi S_r d_s^2 \eta)/(S_i A_r \cos\theta_r), \qquad (4)$$

where d_s is the distance from the surface of the specimen to the radiometer entrance aperture, A_r is the area of the entrance aperture of the radiometer, θ_r is the angle between the incident radiation and the optical axis of the radiometer, and η is the gain factor between the two signals. If the same broadband radiometer/detector is used in the measurement

of the incident and reflected radiation (as is the case in STARR and GOSI, and will be the case in the updated STARR), then the spectral responsivity of the detector need not be considered and $\eta = 1$. Rearranging Eq. (4) and solving for S_r yields

$$S_r = (R/\pi)S_i A_r \cos\theta_r/d_s^2. \tag{5}$$

Suppose $R = 1$ (Lambertian scatterer), $A_r = 1.26\text{E-03 m}^2$ (20 mm aperture radius), $\theta_r = 45$ degrees, and $d_s = 1$ meter. Then

$$S_r/S_i = 2.83\text{E-04}. \tag{6}$$

At 2200 nm, the anticipated flux density is 15 µW/nm (from Table 7). Thus $S_r = 4.24$ nW/nm. This, however, is not the flux density on the detector. It is anticipated that an extended-range InGaAs detector[17] will be used in the SWIR. To reduce noise, the shunt resistance of the detector must be high. The shunt resistance is inversely proportional to the detector area. Therefore the detector will likely have a relatively small diameter, on the order of 3 mm. Such a small size most likely precludes direct imaging of specimen rays onto the detector surface, and thus the detector will be coupled to a small integrating sphere having an entrance port just large enough to set the desired field-of-view when a receiving lens views the specimen at a one meter stand-off distance. The sphere will homogenize the light collected by the radiometer receiver lens, but unfortunately introduces a throughput loss. Let the diameter of the sphere be 3 cm, its entrance port diameter be 1 cm, and the exit port diameter (at which the detector is mounted) be 1.3 cm. Taking into account the reflectance of spectralon, the sphere multiplier, and the transmittance of the receiver lens and detector window, the flux density expected on the detector at 2200 nm is finally calculated to be about 42 pW/nm. In a 14 nm band, the total flux is 588 pW. Compare this result to that in the existing STARR, where the flux at the longest wavelengths is estimated[9] to be < 10 pW.

6. CONCLUSIONS

We describe the design of a system employing a broadband SC fiber laser source coupled to a monochromator that can generate quasi-monochromatic light having a power density more than two orders of magnitude above existing systems that use conventional (QTH) sources. A prototype is currently under construction and this prototype will demonstrate the feasibility of the approach. The ultimate goal of the system is to update and improve the existing national facility for the measurement of BRDF (i.e., STARR) by providing higher signal-to-noise and/or less measurement time required for out-of-plane angle-resolved BRDF measurements into the SWIR. A final design and system will be developed after the prototype results are analyzed and any improvements incorporated. A full uncertainty budget will be developed with the eventual offering of angle-resolved BRDF measurements into the SWIR as a NIST calibration service.

[#]Certain commercial equipment, instruments, software, or materials are identified in this paper to specify the experimental procedure adequately. Such identification is not intended to imply recommendation or endorsement by the National Institute of Standards and Technology, nor is it intended to imply that the materials or equipment identified are necessarily the best available for the purpose.

REFERENCES

[1] Alfano, Robert R., ed. *The Supercontinuum Laser Source: Fundamentals with Updated References.* Springer Science+Business Media Inc., 2006.
[2] Russell, P., "Photonic Crystal Fibers," Science 299, 358-362 (2003).
[3] Wildanger, D., Rittweger, E., Kastrup, L., and Hell, S.W., "STED microscopy with a supercontinuum laser source," Optics Express 16(13), 9614-9621 (2008).
[4] Kaminski, C.F., Watt, R.S., Elder, A.D., Frank, J.H., and Hult, J., "Supercontinuum radiation for applications in chemical sensing and microscopy," Appl. Phys. B 92, 367-378 (2008).
[5] Clowes, J., "Next generation light sources for biomedical applications," Optik & Photonik 1, 36-38 (2008).

[6] Rice, J., Neira, J., Kehoe, M., and Swanson, R., "DMD diffraction measurements to support design of projectors for test and evaluation of multispectral and hyperspectral imaging sensors," Proc. SPIE 7210, 72100D-1-72100D-9 (2009).

[7] Woodward, J.T., Smith, A.W., Jenkins, C.A., Lin, C., Brown, S.W., and Lykke, K.R., "Supercontinuum sources for metrology," Metrologia 46, 1-7 (2009).

[8] Proctor, J.E. and Barnes, P.Y., "NIST high accuracy reference reflectometer-spectrophotometer," J. Res. Natl. Inst. Stand. Technol. 101, 619-627 (1996). See also http://physics.nist.gov/Divisions/Div844/facilities/brdf/starr.html.

[9] Yoon, H.W., Allen, D.W., Eppeldauer, G.P., and Tsai, B.K., "The extension of the NIST BRDF scale from 1100 nm to 2500 nm", Proc. SPIE 7452, 745204 (2009).

[10] Asmail, C.C., Cromer, C.L., Proctor, J.E., and Hsia, J.J., "Instrumentation at the National Institute of Standards and Technology for bidirectional reflectance distribution function (BRDF) measurements," Proc. SPIE 2260, 52-61 (1994). See also http://www.nist.gov/physlab/div844/grp06/scattering_bidirectional.cfm

[11] http://www.fianium.com/supercontinuum.htm

[12] http://www.labsphere.com/data/userFiles/Guide%20to%20IntegratingSphereRadiometry&Photometry.pdf

[13] Gander, M.J. et al, "Measurement of the wavelength dependence of beam divergence for photonic crystal fiber," Optics Letters 24(15) 1017-1019 (1999).

[14] Siegman, A.E., *Lasers.* Mill Valley, University Science Books, 1986.

[15] http://www.zemax.com

[16] http://www.ceramoptec.com/

[17] Yoon, H.W., Dopkiss, M.C., and Eppeldauer, G.P., "Performance comparisons of InGaAs, extended InGaAs, and short-wave HgCdTe detectors between 1 μm and 2.5 μm", Proc. SPIE 6297, 629703 (2006).